

Vacancies in generic Kitaev spin liquids

Ihor Yatsuta and David F. Mross

Department of Condensed Matter Physics, Weizmann Institute of Science, Rehovot 7610001, Israel

(Dated: December 4, 2023)

The Kitaev honeycomb model supports gapless and gapped quantum spin liquid phases. Its exact solvability relies on extensively many locally conserved quantities. Any real-world manifestation of these phases would include imperfections in the form of disorder and interactions that break integrability. We show that the latter qualitatively alters the properties of vacancies in the gapless Kitaev spin liquid: (i) Isolated vacancies carry a magnetic moment, which is absent in the exactly solvable case. (ii) Pairs of vacancies on even/opposite sublattices gap each other with distinct power laws that reveal the presence of emergent gauge flux.

Introduction. Quantum spin liquid (QSL) behavior has been reported for an increasing number of materials [1–7]. These phases are characterized not by their broken symmetries but rather by their fractional quasiparticles and the associated topological properties. QSLs with a bulk gap are sharply distinct from conventional phases by their long-range entanglement. However, this criterion is impractical for experimental identifications, and positively identifying QSLs remains a formidable challenge.

More direct evidence of QSL could arise from gapless (bulk) excitations that respond to weak experimental probes. On the flip side, gapless bulk excitations pose significant challenges for theoretical descriptions. The understanding is primarily derived from poorly-controlled field-theoretical treatments or rather special exactly-solvable models. The best-known example of the latter is the Kitaev honeycomb model [8], whose exact solution relies on its many conserved quantities.

Pioneering work has argued that the highly anisotropic spin-spin interactions of the honeycomb model may arise in strongly spin-orbit coupled Mott insulators. In particular, the honeycomb model is proposed to approximate the local environment experienced by effective spin-1/2 moments in various iridates and α -RuCl₃ (see Refs. [5, 9–22]). The prospect of realizing a Kitaev spin liquid demands a careful analysis of which properties of the finely-tuned toy model are generic and, therefore, constitute predictions for actual experiments. Real materials will inevitably deviate from the honeycomb model in at least two ways [23–25]. Firstly, the many conservation laws are violated, and secondly, there will be disorder.

The implications of the former were analyzed in Refs. [25–29], which showed that generic perturbations qualitatively change key observables without destabilizing the phase. In particular, the honeycomb model exhibits a hard spin gap and ultra-short range spin-spin correlations. By contrast, the spin gap is absent in a generic incarnation of the phase, and correlations decay as power laws [26].

Concurrently, disorder effects were extensively studied for the Kitaev honeycomb model Refs. [30–34]. An important role is played by vacancies, which dominate

the thermodynamic properties at low temperatures and weak magnetic fields. In the gapless phase, an isolated vacancy yields an exact two-fold ground state degeneracy protected by Kramers’ theorem but no moment at zero magnetic field. A weak field induces a moment with a singular field dependence. Moreover, a finite number of vacancies leads to a large number of exact zero-energy states. Ref. 35 constructed a full set of separately conserved Pauli operators for each vacancy, which implies an extensive ground state degeneracy for a finite vacancy concentration. Such a situation is thermodynamically unstable and cannot withstand generic perturbations.

Our work demonstrates that a generic gapless Kitaev QSL with vacancies displays qualitatively different behavior than the fine-tuned honeycomb model. Notably, vacancies exhibit a non-zero magnetic moment at zero field. Such a moment is allowed and could thus be expected on symmetry ground. Indeed, a non-zero moment does arise for each vacancy in the gapped phase of the honeycomb model, which has the same symmetries. Moreover, our work shows that vacancy-induced magnetization falls off according to a universal power law that depends on whether the vacancy traps an emergent \mathbb{Z}_2 gauge flux. Finally, multiple vacancies interact with an RKKY-like interaction characterized by flux-dependent power laws, which lifts the unphysically large ground-state degeneracy of the honeycomb model with vacancies.

Kitaev honeycomb model. To begin, we briefly recall the celebrated Kitaev honeycomb model and its solution. The Hamiltonian is

$$H_K = J \sum_{\mathbf{r}\mathbf{r}'} \sigma_{\mathbf{r}}^{\mu} \sigma_{\mathbf{r}'}^{\mu}, \quad \mathbf{r}' = \mathbf{r} + \hat{e}_{\mu}, \quad (1)$$

where \hat{e}_{μ} with $\mu = x, y, z$ represent the three link directions on a honeycomb lattice. The model H_K exhibits one conserved \mathbb{Z}_2 ‘flux’ $\hat{W}_{\mathcal{O}}$ for any unit cell (see Fig. 1). To express the remaining degrees of freedom, we encode each Pauli operator in four Majorana fermions $\vec{\sigma}_{\mathbf{r}} = i\lambda_{\mathbf{r}}\vec{\xi}_{\mathbf{r}}$ with the local constraint $\mathcal{D}_{\mathbf{r}} \equiv \lambda_{\mathbf{r}}\xi_{\mathbf{r}}^x \xi_{\mathbf{r}}^y \xi_{\mathbf{r}}^z = 1$. The Hamiltonian takes the free-fermion form

$$H_K = -J \sum_{\mathbf{r}\mathbf{r}'} i\lambda_{\mathbf{r}} \hat{u}_{\mathbf{r}\mathbf{r}'} \lambda_{\mathbf{r}'} \quad \hat{u}_{\mathbf{r}\mathbf{r}'} \equiv i\xi_{\mathbf{r}}^{\mu} \xi_{\mathbf{r}'}^{\mu}. \quad (2)$$

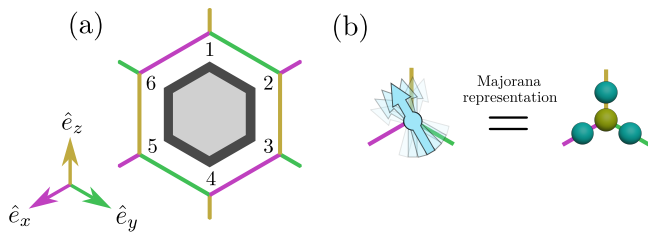


FIG. 1. (a) The honeycomb lattice features three nearest-neighbor link directions, which we denote by $\hat{e}_x, \hat{e}_y, \hat{e}_z$ as indicated. The operators $\hat{W}_\square \equiv \sigma_1^z \sigma_2^x \sigma_3^y \sigma_4^z \sigma_5^x \sigma_6^y$ for any hexagonal plaquette commute with the Kitaev Hamiltonian of Eq. (1). (b) To diagonalize H_K , each spin is represented by four Majorana fermions, subject to a local constraint. It is suggestive to associate three ‘gauge Majoranas’ with the link directions and the remaining ‘matter Majorana’ with the site center.

The link variables $\hat{u}_{\mathbf{r}\mathbf{r}'} = \pm 1$ commute with the Hamiltonian but *anticommute* with the constraints on sites \mathbf{r} and \mathbf{r}' . The fermions $\lambda_{\mathbf{r}}$ likewise anticommute with $\mathcal{D}_{\mathbf{r}}$. Consequently, Eq. (2) describes a \mathbb{Z}_2 gauge theory where the gauge-invariant flux \hat{W}_\square is static. In the ground state, $\hat{W}_\square = 1$ on all plaquettes, and the λ fermions form two Majorana cones at the Brillouin zone corners \mathbf{K}, \mathbf{K}' . At low energies, one may expand near these points via $\lambda_{\mathbf{r}} \sim e^{i\mathbf{K}\cdot\mathbf{r}}\Phi_1(\mathbf{r}) + e^{i\mathbf{K}'\cdot\mathbf{r}}\Phi_2(\mathbf{r})$. The low-energy fermions $\vec{\Phi} = (\Phi_1, \Phi_2)$ are governed by a relativistic Dirac Lagrangian.

Generic Kitaev QSLs. The gapless Kitaev QSL is stable against any weak time-reversal invariant perturbations to H_K . It is useful to distinguish between three kinds of such modifications.

1. *Additional free fermions terms.* Multi-spin interactions such as $\delta H_2 \sim \sigma_1^y \sigma_2^x \sigma_3^y \sigma_4^x = -i\lambda_1 \hat{u}_{12} \hat{u}_{23} \hat{u}_{34} \lambda_4$ (cf. Fig. 1) modify the Majorana band structure. They renormalize the non-universal velocity and change band curvature away from the gapless points, i.e., they contribute irrelevant higher-derivative terms. Despite their simplicity, terms of this type already qualitatively change the properties of vacancies, as we will discuss.

2. *Flux-conserving interactions between λ fermions.* Slightly modified multi-spin terms result in four-fermion interactions, i.e., $\delta H_4 \sim \sigma_1^y \sigma_2^y \sigma_3^x \sigma_4^x = -\lambda_1 \hat{u}_{12} \lambda_2 \lambda_3 \hat{u}_{34} \lambda_4$. In the bulk, they are irrelevant due to the vanishing density of states at the Dirac point. We will show that such terms play an important role when the number of vacancies on two sublattices is unequal.

3. *Flux-changing terms.* The most generic symmetry-allowed interactions, such as the widely studied Heisenberg and Γ terms, fail to commute with \hat{W}_\square , i.e., spoil flux conservation. They render the \mathbb{Z}_2 gauge field dynamical but do not destabilize the phase until the flux gap closes [25–29]. These terms have the most dramatic consequences and qualitatively change bulk observables [26].

Any Kitaev QSL in a real material presumably includes

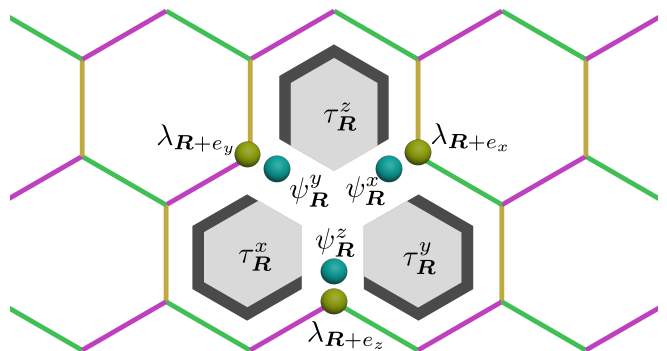


FIG. 2. Removing the site \mathbf{R} affects three hexagonal plaquettes. The corresponding fluxes are reduced to five-spin operators $\tau_{\mathbf{R}}^{x,y,z}$. They are conserved and satisfy the SU(2) algebra Eq. (3). In the fermion representation, one ‘gauge Majorana’ on each of the adjacent sites loses its partner. These dangling Majoranas form a zero-energy subspace and represent the τ operators according to Eq. (4).

all three of these perturbations. In particular, the first two types of contributions will be generated from the last in models that, microscopically, contain only two-spin couplings. Treating them separately allows us to determine the physical origin of various effects, and study them efficiently in large systems. We emphasize that all the effects that we describe relate to quantities that are strictly zero in the honeycomb model without being required to by its global symmetries. As such, including the most generic terms will not bring them back to zero, and our conclusion holds for the general case.

Vacancies in the honeycomb model. To create a vacancy, we now remove the site \mathbf{R} . The three adjacent plaquette operators $W_{\square}^{x,y,z}$ are also affected: Removing $\vec{\sigma}_{\mathbf{R}}$ yields three conserved five-spin operators $\tau_{\mathbf{R}}^\mu = \sigma_{\mathbf{R}}^\mu W_{\square}^\mu$. However, they do not mutually commute. Instead, they satisfy the SU(2) algebra

$$[\tau_{\mathbf{R}}^\mu, \tau_{\mathbf{R}}^\nu] = 2i\epsilon^{\mu\nu\kappa} \tau_{\mathbf{R}}^\kappa W_{\square}, \quad (3)$$

with $W_{\square} = \pm 1$ conserved flux around the vacancy site [35]. The τ operators associated with different vacancies are independent and commute. Consequently, the exact ground state degeneracy is bounded as $g \geq 2^N$.

The actual degeneracy is significantly larger, which is the first result of this work. To obtain it, we note that removing the \mathbf{R} site strips three ξ fermions on the adjacent sites of their partner. We denote them by $\psi_{\mathbf{R}}^\mu$. Additionally, there is an exact zero-energy mode $\psi_{\mathbf{R}}^0$ for the λ fermions on the sublattice opposite to that of the vacancy. For any gauge choice of the link variables $\hat{u}_{\mathbf{r}\mathbf{r}'} = \pm 1$, the four zero energy modes $\psi_{\mathbf{R}}^{0,x,y,z}$ satisfy

$$\vec{\tau}_{\mathbf{R}} = \pm \frac{i}{2} \vec{\psi}_{\mathbf{R}} \times \vec{\psi}_{\mathbf{R}}, \quad \psi_{\mathbf{R}}^0 \psi_{\mathbf{R}}^x \psi_{\mathbf{R}}^y \psi_{\mathbf{R}}^z = \pm 1. \quad (4)$$

The signs in both expressions are not gauge invariant, but they are unimportant for our purposes. For N_A and N_B

vacancies on the two sublattices, there are $4(N_A + N_B)$ fermions $\psi_{\mathbf{R}_i}^\mu$ subject to a single constraint. However, not all $\psi_{\mathbf{R}_i}^0$ represent zero-energy modes; they hybridize pairwise when occupying opposite sublattices. As such, we find that the degeneracy is

$$g_K = 2^{N_A + N_B + \max(N_A, N_B) - 1}, \quad (5)$$

which is parametrically larger than the bound obtained by counting $\vec{\tau}$ operators. A source of additional degeneracies are open strings of spin operators that connect two vacancies. Such strings commute with all W_\square , $\vec{\tau}$ and are time-reversal odd for vacancies on the same sublattice.

To conclude the summary of vacancies in H_K , we consider the vacancy-induced moment. Any $\sigma_{\mathbf{r}}$ not adjacent to a vacancy anti-commutes with some of the W_\square and thus has zero expectation value. By contrast, $\sigma_{\mathbf{R} + \hat{e}_\mu}^\mu = i\lambda_{\mathbf{R} + \hat{e}_\mu} \psi_{\mathbf{R}}^\mu$ commute with all remaining W_\square and could thus acquire a non-zero value in the ground state manifold. Projecting these operators into the degenerate subspace yields

$$P\sigma_{\mathbf{R} + \hat{e}_\mu}^\mu P = i\mathcal{N}_{\mathbf{R} + \hat{e}_\mu}^0 \psi_{\mathbf{R}}^0 \psi_{\mathbf{R}}^\mu = \mathcal{N}_{\mathbf{R} + \hat{e}_\mu}^0 \tau_{\mathbf{R}}^\mu. \quad (6)$$

Here, $\mathcal{N}_{\mathbf{r}}^0$ is the amplitude of the delocalized zero-mode wave function on the site \mathbf{r} . In the gapless QSL, the zero mode is not normalizable, and $\lim_{L \rightarrow \infty} \mathcal{N}^0(L) = 0$. Consequently, there is no magnetic moment, although the ‘phantom spin’ τ , which has the same global symmetries, has unit magnitude.

When the flux around the vacancy is $W_\square = 1$, the zero-mode wave function decays as $1/r$, [31, 36] and the normalization is $\mathcal{N}_0 \sim (\log L)^{-1/2}$. A weak magnetic field h represents a length scale $L_h \sim 1/h$, hence, for $L_h \ll L$, the magnetization becomes $m(h) \sim (\log h)^{-1/2}$, as found in Ref. [30]. For $W_\square = -1$, the zero mode is localized even more poorly. In either case, the zero-mode amplitude and the vacancy-induced moment are zero in the thermodynamic limit.

Single vacancy in a generic Kitaev QSL. When the honeycomb model H_K of Eq. (1) is perturbed by generic interactions, the behavior of vacancies changes qualitatively. Most significantly, the phantom spins are revealed, and vacancies exhibit a non-zero magnetic moment, which could be observed experimentally. To demonstrate this feature, we consider the local coupling

$$H_{\sigma\tau} = g \sum_{\mu} \tau_{\mathbf{R}}^\mu \sigma_{\mathbf{R} + \hat{e}_\mu}^\mu, \quad (7)$$

which preserves the global symmetries of the honeycomb model. It corresponds to a six-spin interaction, which is unlikely to be realized microscopically. Still, it will be generated by generic two-spin terms and must, therefore, be included in the low-energy theory. The analysis of $H = H_K + H_{\sigma\tau}$ is straightforward: We note that H commutes with all flux operators \hat{W} and with $\tau_{\mathbf{R}}^\mu$. Consequently, any state in the two-fold degenerate ground

state manifold corresponds to a specific orientation of the vector $\vec{\tau}_{\mathbf{R}}$ on the Bloch sphere. For any choice of this direction, $H_{\sigma\tau}$ amounts to a Zeeman magnetic field near the vacancy, which induces a non-zero moment, as discussed above.

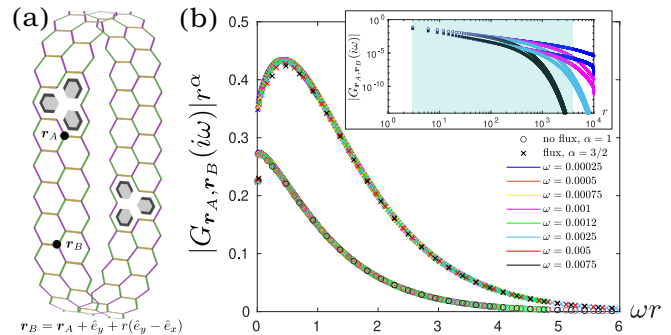


FIG. 3. Trapped fluxes modify the scaling behavior of the fermion Green function. We numerically computed the Green function on an infinite cylinder with vacancies on opposite sites. Their separation is $L = 10^4$ unit cells. One coordinate is at a fixed position near a vacancy, and the second is varied, as indicated in (a). For $1 \ll r, \omega^{-1} \ll L$ the data collapse onto the scaling of Eq. (10) with $z = 1$ and $\alpha = 1$ or $\alpha = 3/2$, depending on the trapped flux (b). A double-logarithmic plot of the bare Green functions is shown in the inset. The shaded region indicates the data range used in the collapse.

The toy model provides a useful proof of principle that generic vacancies are associated with a non-zero magnetic moment. To compute the magnetization profile in a generic situation, we follow the perturbative approach of Ref. [26]. It demonstrated that the magnetization acquires a contribution from the flux-conserving operator $\delta\sigma_{\mathbf{r}}^\mu \sim i f_{\mathbf{r}\mathbf{r}'\mathbf{r}''}^\mu \lambda_{\mathbf{r}'} \lambda_{\mathbf{r}''}$, with \mathbf{r}' , \mathbf{r}'' on the same sublattice. This contribution is absent in the original honeycomb model H_K but dominates the long-wavelength behavior in the generic case. Additionally, the ‘vacancy-Majoranas’ ψ of Eq. (4) can couple linearly to the λ via

$$H_{\psi\lambda} = it \sum_{\mu} \psi_{\mathbf{R}}^\mu \lambda_{\mathbf{R}_\mu}. \quad (8)$$

Here \mathbf{r}_μ can be any site on the same sublattice as the vacancy. (It is conceptually simplest, but not necessary, to take $\mathbf{R}_{x,y,z}$ all different, e.g., by the choice $\mathbf{R}_\mu = \mathbf{R} + 3\hat{e}_\mu$). At the second order in t and the first order in f , the magnetization at \mathbf{r} is given by

$$\langle \sigma_{\mathbf{r}} \rangle \propto \int d\omega G_{\mathbf{r}, \mathbf{R}_\mu}(\omega) G_{\mathbf{r}', \mathbf{R}_\mu}(-\omega) \langle \tau_{\mathbf{R}} \rangle. \quad (9)$$

The Green function $G_{\mathbf{r}, \mathbf{r}'}(\omega) \equiv \langle i\lambda_{\mathbf{r}} \lambda_{\mathbf{r}'} \rangle_\omega$ at long distances follows the scaling

$$G_{\mathbf{r}, \mathbf{r}'}(\omega) \sim \omega^\alpha F(\omega |\mathbf{r} - \mathbf{r}'|^z). \quad (10)$$

Without vacancies, the exponents are $z = \alpha = 1$, and the scaling function F is a modified Bessel function. When

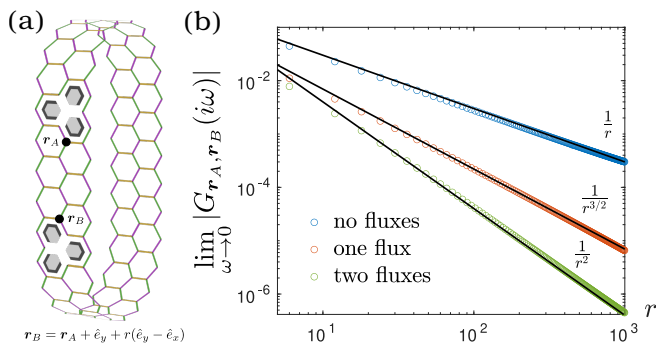


FIG. 4. The free-fermion Green functions between the sites adjacent to two vacancies decay with power laws that depend on the trapped fluxes. We computed them numerically for an infinite cylinder with $L = 10^4$ unit cells in circumference and for the frequency $\omega = 10^{-8} \ll L^{-1}$. The vacancy locations are shown in (a); we increase their separation in steps of three unit cells, the periodicity due to the Dirac points' location (see App. B for details). For all three flux configurations we find distinct power laws, shown in the logarithmic scale in (b). The shown data corresponds to $r = 0 \pmod{3}$ distances between the two sites.

either \mathbf{r} or \mathbf{r}' is near a vacancy, the scaling is modified depending on the flux at the vacancy. By solving the free-fermion system numerically, we find that $z = 1$ remains unchanged. The exponent α remains unity in the absence of flux but changes to $\alpha^{\text{flux}} = 3/2$ in its presence, see Fig. 3. Consequently we find $\sigma_{\mathbf{r}} \sim |\mathbf{r}|^{-3}$ and $\sigma_{\mathbf{r}'} \sim |\mathbf{r}'|^{-4}$ for $W_{\triangle} = +1$ and $W_{\triangle} = -1$, respectively. Remarkably, the magnetization around a vacancy can be used to determine the presence of a trapped flux.

Multiple vacancies in a generic Kitaev QSL. We now consider two well-isolated vacancies on opposite sublattices. The delocalized would-be zero-modes hybridize in this case, and the ground state manifold is spanned by the dangling modes alone. They are subject to the constraint $\psi_{\mathbf{R}}^x \psi_{\mathbf{R}'}^y \psi_{\mathbf{R}''}^z \psi_{\mathbf{R}'''}^x \psi_{\mathbf{R}''''}^y \psi_{\mathbf{R}'''''}^z = \pm i$, depending on the choice of the link variables \hat{u} . The constraint implies that $\tau_{\mathbf{R}}^{\mu} \tau_{\mathbf{R}'}^{\nu} = \pm i \psi_{\mathbf{R}}^{\mu} \psi_{\mathbf{R}'}^{\nu}$, i.e., the interaction between phantom spins is a fermion bilinear. When the dangling modes hybridize with the bulk fermions via $H_{\psi\lambda}$ of Eq. (8), the phantom spins experience an effective coupling

$$\delta H_{\tau\tau}^{AB} = t^2 G_{\mathbf{R}_{\mu}, \mathbf{R}'_{\nu}}(\omega = 0) \tau_{\mathbf{R}}^{\mu} \tau_{\mathbf{R}'}^{\nu}. \quad (11)$$

Notice that this RKKY-like interaction is mediated by a single fermion, unlike its analog in conventional metals, where it arises from particle-hole pairs. Similar to the single-vacancy case, the Green function depends on the fluxes at the vacancies. We numerically computed it for free fermions on an infinite cylinder. Our results show distinct power laws (Fig. 4). The Green function decays as $G \sim R^{-1}$, $R^{-3/2}$, or R^{-2} for trapped fluxes at neither, one, or both vacancies, respectively.

When two vacancies are on the same sublattice, their delocalized zero modes are protected from hybridizing.

Indeed, *any* bilinear of ψ fermions is odd under time-reversal symmetry in this case. Still, interactions such as Eq. (7) with $PH_{\sigma\tau}P \propto \psi_{\mathbf{R}}^x \psi_{\mathbf{R}}^y \psi_{\mathbf{R}}^z \psi_{\mathbf{R}}^0$ can reduce the ground state degeneracy to the one encoded by the phantom spins $\vec{\tau}_{\mathbf{R}}, \vec{\tau}_{\mathbf{R}'}$. These, in turn, can interact via a more conventional RKKY-like interaction

$$\delta H_{\tau\tau}^{AA} \propto \tau_{\mathbf{R}}^{\mu} \tau_{\mathbf{R}'}^{\mu'} \times \int_{\omega} G_{\mathbf{R}_{\kappa}, \mathbf{R}'_{\kappa'}}(\omega) G_{\mathbf{R}_{\nu}, \mathbf{R}'_{\nu'}}(-\omega), \quad (12)$$

when ψ are coupled to the bulk via Eq. (8). Based on the scaling determined above, we conclude that the interaction decays as R^{-3} , R^{-4} or R^{-5} , depending on W_{\triangle} at either vacancy.

To support our perturbative analysis, we used exact diagonalization on a 24-site cluster with two vacancies. When the vacancies are on opposite sublattices, we observed that perturbing $H_{\mathbf{K}}$ with the free-fermion term of Eq. (8) is sufficient to obtain a unique ground state. By contrast, for vacancies on the same sublattice, the same term does not reduce the eight-fold ground-state degeneracy. Further including the four-fermion coupling Eq. (7) lifts this degeneracy, as we predicted. Additionally, we confirmed that the Kitaev- Γ -Heisenberg model [23–25] has a unique ground state in both cases.

Discussion. We have shown that generic, symmetry-preserving perturbations to the honeycomb model qualitatively change the properties of vacancies. Notably, isolated vacancies display a non-zero magnetic moment, which could be measured using sensitive magnetometric tools like superconducting quantum interference devices (SQUIDS). Similarly, the bulk magnetic susceptibility χ for a finite vacancy concentration n_{imp} is significantly modified. For magnetic fields $h \gg \sqrt{n_{\text{imp}}}$, the presence of vacancies in the honeycomb model gives rise to a weakly singular contribution to the magnetic susceptibility characterized by $\chi_{\text{imp}}(h) \sim n_{\text{imp}} \log(h)$ [31]. In contrast, we predict that a generic Kitaev QSL exhibits field-independent magnetization under these conditions. We expect the weak-field limit to display rich physics depending on the vacancy distribution, which would be an interesting topic for future studies.

Vacancies in spin liquids are closely related to magnetic impurities, i.e., Kondo-type models [35, 37, 38]. Our findings regarding how scaling is altered by flux excitations bear direct implications for the RKKY interaction [35]. Furthermore, the interactions among vacancies in a generic spin liquid may give rise to intriguing multi-impurity Kondo phenomena [39, 40]. Given that vacancy-vacancy couplings already manifest at the Gaussian level [cf. Eq. (11)], it would even be possible to explore them numerically using a free-fermion bath.

Acknowledgments. It is a pleasure to acknowledge illuminating conversations with Jason Alicea and Elio König. This work was supported by the Israel Science Foundation (ISF) under grant 2572/21 and by the Minerva Foundation with funding from the Federal German

Ministry for Education and Research.

-
- [1] L. Balents, *Nature* **464**, 199 (2010).
- [2] L. Savary and L. Balents, *Reports on Progress in Physics* **80**, 016502 (2016).
- [3] M. R. Norman, *Rev. Mod. Phys.* **88**, 041002 (2016).
- [4] Y. Zhou, K. Kanoda, and T.-K. Ng, *Rev. Mod. Phys.* **89**, 025003 (2017).
- [5] H. Takagi, T. Takayama, G. Jackeli, G. Khaliullin, and S. E. Nagler, *Nature Reviews Physics* **1**, 264 (2019).
- [6] J. Knolle and R. Moessner, *Annu. Rev. Condens. Matter Phys.* **10**, 451 (2019).
- [7] C. Broholm, R. J. Cava, S. A. Kivelson, D. G. Nocera, M. R. Norman, and T. Senthil, *Science* **367**, eaay0668 (2020).
- [8] A. Kitaev, *Annals of Physics* **321**, 2 (2006), january Special Issue.
- [9] A. Banerjee, C. A. Bridges, J. Q. Yan, A. A. Aczel, L. Li, M. B. Stone, G. E. Granroth, M. D. Lumsden, Y. Yiu, J. Knolle, S. Bhattacharjee, D. L. Kovrizhin, R. Moessner, D. A. Tennant, D. G. Mandrus, and S. E. Nagler, *Nature Materials* **15**, 733 (2016).
- [10] S. M. Winter, A. A. Tsirlin, M. Daghofer, J. van den Brink, Y. Singh, P. Gegenwart, and R. Valentí, *Journal of Physics: Condensed Matter* **29**, 493002 (2017).
- [11] M. Hermanns, I. Kimchi, and J. Knolle, *Annual Review of Condensed Matter Physics* **9**, 17 (2018).
- [12] Y. Motome and J. Nasu, *Journal of the Physical Society of Japan* **89**, 012002 (2020).
- [13] S. Trebst and C. Hickey, *Physics Reports* **950**, 1 (2022), kitaev materials.
- [14] Y. Kasahara, T. Ohnishi, Y. Mizukami, O. Tanaka, S. Ma, K. Sugii, N. Kurita, H. Tanaka, J. Nasu, Y. Motome, T. Shibauchi, and Y. Matsuda, *Nature (London)* **559**, 227 (2018).
- [15] K. Kitagawa, T. Takayama, Y. Matsumoto, A. Kato, R. Takano, Y. Kishimoto, S. Bette, R. Dinnebier, G. Jackeli, and H. Takagi, *Nature (London)* **554**, 341 (2018).
- [16] S. K. Takahashi, J. Wang, A. Arsenault, T. Imai, M. Abramchuk, F. Tafti, and P. M. Singer, *Phys. Rev. X* **9**, 031047 (2019).
- [17] M. G. Yamada, *npj Quantum Materials* **5**, 82 (2020).
- [18] S.-H. Do, C. H. Lee, T. Kihara, Y. S. Choi, S. Yoon, K. Kim, H. Cheong, W.-T. Chen, F. Chou, H. Nojiri, and K.-Y. Choi, *Phys. Rev. Lett.* **124**, 047204 (2020).
- [19] T. Yokoi, S. Ma, Y. Kasahara, S. Kasahara, T. Shibauchi, N. Kurita, H. Tanaka, J. Nasu, Y. Motome, C. Hickey, S. Trebst, and Y. Matsuda, *Science* **373**, 568 (2021).
- [20] J. A. N. Bruin, R. R. Claus, Y. Matsumoto, N. Kurita, H. Tanaka, and H. Takagi, *Nature Physics* **18**, 401 (2022).
- [21] P. Czajka, T. Gao, M. Hirschberger, P. Lampen-Kelley, A. Banerjee, J. Yan, D. G. Mandrus, S. E. Nagler, and N. P. Ong, *Nature Physics* **17**, 915 (2021).
- [22] P. Czajka, T. Gao, M. Hirschberger, P. Lampen-Kelley, A. Banerjee, N. Quirk, D. G. Mandrus, S. E. Nagler, and N. P. Ong, *Nature Materials* **22**, 36 (2023).
- [23] J. c. v. Chaloupka, G. Jackeli, and G. Khaliullin, *Phys. Rev. Lett.* **105**, 027204 (2010).
- [24] J. G. Rau, E. K.-H. Lee, and H.-Y. Kee, *Phys. Rev. Lett.* **112**, 077204 (2014).
- [25] J. c. v. Chaloupka, G. Jackeli, and G. Khaliullin, *Phys. Rev. Lett.* **110**, 097204 (2013).
- [26] X.-Y. Song, Y.-Z. You, and L. Balents, *Phys. Rev. Lett.* **117**, 037209 (2016).
- [27] D. Gotfryd, J. Rusnačko, K. Wohlfeld, G. Jackeli, J. c. v. Chaloupka, and A. M. Oleś, *Phys. Rev. B* **95**, 024426 (2017).
- [28] M. Gohlke, R. Verresen, R. Moessner, and F. Pollmann, *Phys. Rev. Lett.* **119**, 157203 (2017).
- [29] S.-S. Zhang, G. B. Halász, W. Zhu, and C. D. Batista, *Phys. Rev. B* **104**, 014411 (2021).
- [30] A. J. Willans, J. T. Chalker, and R. Moessner, *Phys. Rev. Lett.* **104**, 237203 (2010).
- [31] A. J. Willans, J. T. Chalker, and R. Moessner, *Phys. Rev. B* , 115146 (2011).
- [32] G. J. Sreejith, S. Bhattacharjee, and R. Moessner, *Phys. Rev. B* **93**, 064433 (2016).
- [33] J. Nasu and Y. Motome, *Phys. Rev. B* **102**, 054437 (2020).
- [34] W.-H. Kao, J. Knolle, G. B. Halász, R. Moessner, and N. B. Perkins, *Phys. Rev. X* **11**, 011034 (2021).
- [35] K. Dhochak, R. Shankar, and V. Tripathi, *Phys. Rev. Lett.* **105**, 117201 (2010).
- [36] V. M. Pereira, F. Guinea, J. M. B. Lopes dos Santos, N. M. R. Peres, and A. H. Castro Neto, *Phys. Rev. Lett.* **96**, 036801 (2006).
- [37] M. Vojta, A. K. Mitchell, and F. Zschocke, *Phys. Rev. Lett.* **117**, 037202 (2016).
- [38] S. D. Das, K. Dhochak, and V. Tripathi, *Phys. Rev. B* **94**, 024411 (2016).
- [39] C. Jayaprakash, H. R. Krishna-murthy, and J. W. Wilkins, *Phys. Rev. Lett.* **47**, 737 (1981).
- [40] B. A. Jones and C. M. Varma, *Phys. Rev. Lett.* **58**, 843 (1987).
- [41] V. M. Pereira, J. M. B. Lopes dos Santos, and A. H. Castro Neto, *Phys. Rev. B* **77**, 115109 (2008).

Appendix A: The Green function of a honeycomb lattice on an infinite cylinder with defects

In the main text, we are interested in the Green functions for a honeycomb lattice with vacancies or flux excitations. To obtain them efficiently, we split the system into a single chain ($x = 0$ in Fig. 5) and semi-infinite baths on either side of it. The former contains all defects; the latter are translation invariant in the periodic direction. The Green function on the central region is then given by

$$G(i\omega) = [i\omega - H^{\text{center}} - \Sigma(i\omega)]^{-1}, \quad (\text{A1})$$

where H^{center} is the Hamiltonian for the central cylinder. The self-energy $\Sigma(i\omega)$ is determined by the Green function $G_{\text{bath}}(i\omega)$ of the semi-infinite bath via

$$\Sigma(i\omega) = H^{\text{center-bath}} G_{\text{bath}}(i\omega) H^{\text{bath-center}}, \quad (\text{A2})$$

where $H^{\text{center-bath}}$ contains any elements that connect the central cylinder to the bath. Crucially, an analytical expression for the relevant elements of G_{bath} can be easily

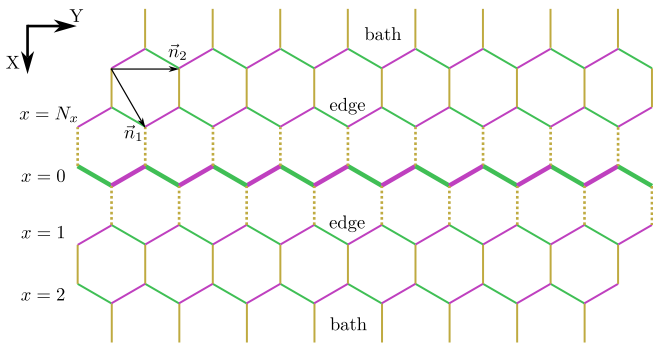


FIG. 5. We treat the two-dimensional honeycomb lattice as a one-dimensional chain coupled to a two-dimensional bath. The former contains all $x = 0$ sites and is indicated by thick links. Thin links indicate couplings within the bath, and dotted lines are the chain-bath couplings. The separation into chain and bath is purely formal; the values of all nearest-neighbor couplings are identical. We perform our numerical calculations on an infinite cylinder with \vec{n}_2 the periodic direction.

obtained for any momentum k_y in the periodic direction. Inserting the thus-obtained $\Sigma(i\omega)$ into Eq. (A1) yields the full Green function $G(i\omega)$ of the central region. In essence, the calculation of $G(i\omega)$ reduces to solving an effective quasi-one-dimensional model.

To obtain the bath Green function, we begin with an infinite cylinder that is translation invariant in both directions. Its Green function G^0 is given by

$$G_{\mathbf{k}}^0(i\omega) = -\frac{1}{\omega^2 + |g(\mathbf{k})|^2} \begin{pmatrix} i\omega & ig(\mathbf{k}) \\ -ig^*(\mathbf{k}) & i\omega \end{pmatrix}, \quad (\text{A3})$$

$$g(\mathbf{k}) = 1 + e^{ik_x} + e^{ik_y}. \quad (\text{A4})$$

To obtain the semi-infinite bath, we add a potential barrier V for all $x = 0$ (say) and compute the new Green function from $G = [G^0 + V]^{-1}$. Taking $V \rightarrow \infty$, we thus obtain

$$G_{x,x'}^{\text{bath}}(k_y) = G_{x,x'}^0(k_y) - \frac{G_{x,0}^0(k_y)G_{0,x'}^0(k_y)}{G_{0,0}^0(k_y)}. \quad (\text{A5})$$

For Eq. A2 with $H^{\text{center-bath}}$, which only contains nearest-neighbor hopping, we only need $G_{1,1}^{\text{bath}}(k_y)$, for which we find

$$G_{1,1}^{\text{bath}}(k_y) = i \left(\frac{1 + \omega^2 + 2 \cos(k_y)}{2\omega} \right) - i \left(\frac{\sqrt{8[\omega^2 + \cos(k_y)] \cos^2(k_y/2) + (1 + \omega^2)^2}}{2\omega} \right). \quad (\text{A6})$$

Appendix B: Two vacancies on a honeycomb lattice

It is well-known that vacancies on the same sublattice provide independent zero modes, while zero modes of the

vacancies on opposite sublattices can hybridize [41]. The strength of this hybridization, and thus the degree to which the degeneracy is lifted, depends sensitively on the relative location of the two vacancies. To understand this property, we compute the matrix element

$$M_{\mathbf{R}_A, \mathbf{R}_B} \equiv \sum_{\mathbf{r}, \mathbf{r}'} \Psi_{\mathbf{R}_A}^*(\mathbf{r}) H_{\mathbf{R}_A, \mathbf{R}_B}(\mathbf{r}, \mathbf{r}') \Psi_{\mathbf{R}_B}(\mathbf{r}'), \quad (\text{B1})$$

where $\Psi_{\mathbf{R}}(\mathbf{r}')$ is the zero-mode wave function for a honeycomb lattice with a single vacancy and $H_{\mathbf{R}_A, \mathbf{R}_B}$ is the Hamiltonian of the same system with two vacancies. Since $\Psi_{\mathbf{R}}(\mathbf{r}')$ is an exact zero-mode of the single-vacancy model

$$H_{\mathbf{R}_B} = H_{\mathbf{R}_A, \mathbf{R}_B} - iJ \sum_{\mu=x,y,z} |\mathbf{R}_A\rangle \langle \mathbf{R}_A + \hat{e}_\mu| \quad (\text{B2})$$

$$+ iJ \sum_{\mu=x,y,z} |\mathbf{R}_A + \hat{e}_\mu\rangle \langle \mathbf{R}_A|, \quad (\text{B3})$$

we can simplify

$$M_{\mathbf{R}_A, \mathbf{R}_B} = -iJ \sum_{\mu=x,y,z} \Psi_{\mathbf{R}_A}^*(\mathbf{R}_A + \hat{e}_\mu) \Psi_{\mathbf{R}_B}(\mathbf{R}_A). \quad (\text{B4})$$

To understand the behavior of $M_{\mathbf{R}_A, \mathbf{R}_B}$, it is thus sufficient to look at $\Psi_{\mathbf{R}_B}(\mathbf{R}_A)$, which was computed in Ref. [36]. For $\mathbf{R}_A = \mathbf{R}_B - \hat{e}_y - n(\hat{e}_y - \hat{e}_x)$, we find

$$\lim_{n \rightarrow \infty} |\Psi_{\mathbf{R}_B}(\mathbf{R}_A)| \sim \begin{cases} \frac{1}{n} & n = 0 \pmod{3}, \\ \frac{1}{n} & n = 2 \pmod{3}, \\ \frac{1}{n^2} & n = 1 \pmod{3}. \end{cases} \quad (\text{B5})$$

For the first two cases, the smallest hybridization in a finite system is parameterically the same as the finite-size splitting for the bulk modes. As such, they do not substantially modify the low-energy Green function. By contrast, in the third case, the energy of the nearly-zero modes $(\Psi_{\mathbf{R}_A} \pm i\Psi_{\mathbf{R}_B})/\sqrt{2}$ is parameterically smaller and will dominate the low-energy Green function. As this property relies on a careful cancellation between different $1/n$ contributions, we deem it less generic and focus on the other cases in the main text.

1. Anomalous low-energy modes for specific vacancy location

To confirm the behavior derived above, we numerically computed the spectrum for systems of size $N_x = N_y = 8 + 6k + 1$ and $N_x = N_y = 6 + 6k + 1$, $k \in \mathbb{Z}$, which support periodic $n = 1 \pmod{3}$ and $n = 0 \pmod{3}$ subsequences along the y direction, respectively. We place two vacancies along the chain $x = \text{const}$ and separate them by $N_y/2$ unit cells such that the distance between the vacancy sites belongs to the corresponding subsequence.

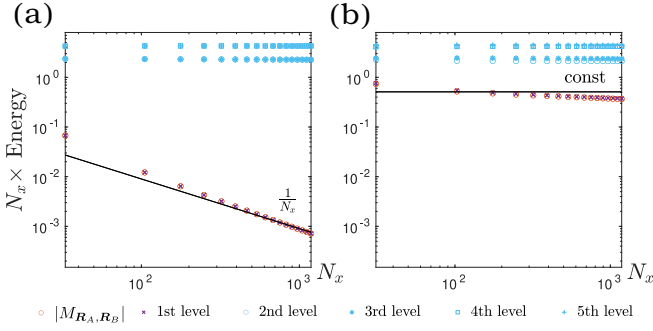


FIG. 6. The energies of the first five energy levels as functions of the system size when the distance between the vacancies is approximately $N_y/2$. The columns (a) and (b) correspond to the $n = 1 \bmod 3$ and $n = 0 \bmod 3$ distances, respectively. The orange circles show the amplitude $M_{\mathbf{R}_A, \mathbf{R}_B}$. The power laws with definite powers (the solid black lines) are put as reference lines to illustrate the lowest energy state dependence.

For $n = 1 \bmod 3$, the lowest energy state occurs well separated from all other states; its energy decays parametrically differently with vacancy separation (see Fig. 6). The lowest energy state agrees with the matrix element $|M_{\mathbf{R}_A, \mathbf{R}_B}|$ within a relative error of less than a few percent when $|\vec{r}_{v1} - \vec{r}_{v2}| \gg 1$, which indicates the zero mode origin of that state. We note that the lowest energy state in either case does not strictly follow the suggested power law. These deviations arise due to the zero-mode normalization factors, which decay logarithmically with system size.

In the presence of anomalous low-energy modes, the Green functions change qualitatively. Fig. 7 (a) and (b) show the Green function without and with such modes, respectively. In the latter case, it does not follow a clear power law. When either vacancy traps a flux, there are no anomalous low-energy states for any vacancy separation. In those cases, the Green functions decay with identical power laws for all sequences.

Appendix C: Exact diagonalization of a 24-site cluster with two vacancies

To verify the predicted lifting of degeneracies, we performed exact diagonalization of a 24-site cluster with two vacancies on equal or opposite sublattices (See Fig. 8). We computed energy spectra for

$$H_1 = H_{\text{K,anis}} + H_{\text{quad}} \quad (\text{C1})$$

$$H_2 = H_{\text{K,anis}} + H_{\text{quad}} + H_{\text{quart}} \quad (\text{C2})$$

$$H_3 = H_{\text{K,anis}} + H_{\text{Heis.-}\Gamma} \quad (\text{C3})$$

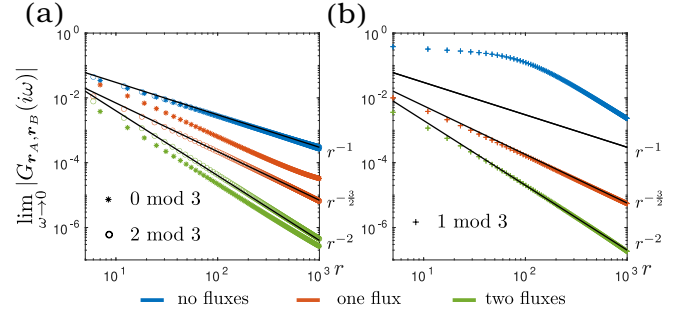


FIG. 7. Green functions between the sites adjacent to two vacancies separated along the periodic direction of an infinite cylinder with a 10000 unit cell circumference. For vacancy separations given by $n = 0 \bmod 3$ or $n = 2 \bmod 3$ unit cells, we find clear power laws that depend on the presence of fluxes at the vacancies (a). For separations $n = 1 \bmod 3$, the Green functions follow a qualitatively different decay when neither vacancy traps flux (b). When either of them traps a flux, we recover the same power-law decay as in (a).

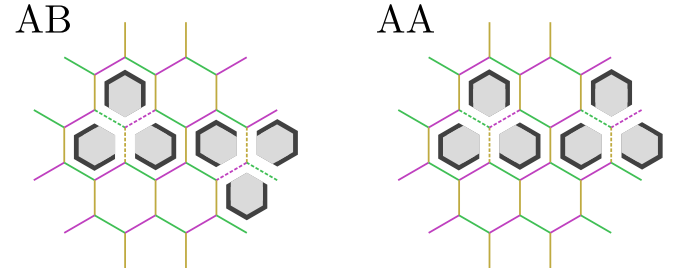


FIG. 8. Two vacancies in the 24-site cluster. The dotted lines and five-spin τ operators indicate the vacancy sites. The external lines of the same color show how the cluster is periodically connected.

with

$$H_{\text{K,anis}} = \sum_{\mathbf{r}, \mu} J^\mu \sigma_{\mathbf{r}}^\mu \sigma_{\mathbf{r}+\hat{e}_\mu}^\mu \quad (\text{C4})$$

$$H_{\text{quad}} = \frac{J_{\text{quad}}}{2} \sum_{\mathbf{R}, \mu \neq \kappa \neq \nu} (1 + \epsilon_{\mu\nu\kappa}) \sigma_{\mathbf{R}+\hat{e}_\mu}^\kappa \sigma_{\mathbf{R}+\hat{e}_\mu+\hat{e}_\nu}^\nu \quad (\text{C5})$$

$$H_{\text{quart}} = J_{\text{quart}} \sum_{\mathbf{R}, \alpha} \sigma_{\mathbf{R}+\hat{e}_\alpha} \tau_{\mathbf{R}}^\alpha \quad (\text{C6})$$

$$H_{\text{Heis.}-\Gamma} = J_{\text{Heis.}-\Gamma} \sum_{\langle \mathbf{r} \mathbf{r}' \rangle} \sigma_{\mathbf{r}} \cdot \sigma_{\mathbf{r}'} \quad (\text{C7})$$

$$H_{\Gamma} = J_{\text{Heis.}-\Gamma} \sum_{\mathbf{r}, \mu} |\epsilon_{\mu\nu\kappa}| \sigma_{\mathbf{r}}^\nu \sigma_{\mathbf{r}+\hat{e}_\mu}^\kappa \quad (\text{C8})$$

Anisotropic Kitaev couplings ($J_z \neq J_x, J_y$) are important for the AA case, where the positions of the vacancies that preserve global spatial symmetries partially protect degeneracies.

Our results are summarized in Fig. 9. They confirm our expectations that the ground state of generic KSL with vacancies is unique. We observed similar behavior

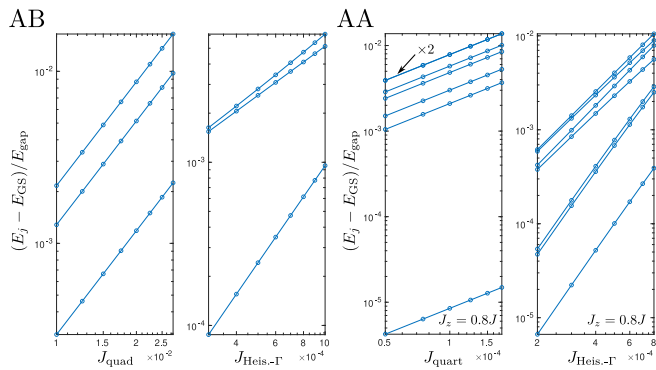


FIG. 9. The energy differences $(E_j - E_{\text{GS}})/E_{\text{gap}}$ between the first 3 (or the first 7 in the AA case) excited states and the ground state as functions of different coupling strengths. E_{gap} is the energy of the 4th (or the 8th in the AA case) excited state. In the AA case with quartic interactions, the 6th and 7th excited states have close energies indistinguishable in the plot. The energy difference changes as a power law with a fixed power for flux-preserving interactions. When interactions mix flux sectors, different energy levels may have different scaling dependences.

on a 28-site cluster where two vacancies can be fully separated. In that case, only the AA case with quartic terms requires anisotropy for full degeneracy lifting.